Nonlinear viscosity law in FE analysis of high damping rubber bearings and expansion joints

A.F.M.S. Amin[1], A.R. Bhuiyan[2], T. Hossain[3], Y. Okui[4]

[1]Department of Civil Engineering, Bangladesh University of Engineering and Technology, Dhaka-1000, Bangladesh

[2]Department of Civil Engineering, Chittagong University of Engineering and Technology, Chittagong 4349, Bangladesh

[3]Department of Civil Engineering, Dhaka University of Engineering and Technology, Gazipur 1700, Bangladesh

[4]Department of Civil and Environmental Engineering, Saitama University, 255 Shimo Okubo, Sakura-ku, Saitama 338-8570, Japan

Abstract

A simple computational strategy for FE implementation of a finite strain visco-hyperelasticity model for rubber-like materials is developed. The constitutive model bears strong physical significance due to the explicit consideration of nonlinear dependence of viscosity through internal variables e.g. past maximum overstress and current deformation. To simulate the stress-strain response for particular one dimensional boundary value problems, a scheme for solving the first order differential equation representing the viscosity induced strain-rate effect of rubber is proposed. The

[1] Corresponding author: Email: samin@ce.buet.ac.bd; Telephone: +88028616833 Ext. 7944; Fax: +88029665639

scheme was successful in reproducing experimental results obtained from high damping rubber specimens. In addition, the wider applicability of the proposed strategy in simulation was tested by verifying the numerical results with independent experiments on full scale high damping rubber bearings of different geometry and loading rate. The effect of shape factor on bearing responses is examined through numerical examples obtained from different FE models subjected to the same load and loading rate. Finally, the proposed computational strategy is applied to locate the regions of stress concentrations in a steel plate laminated rubber expansion joints used widely to transfer reactions at central hinge locations of balanced cantilever highway bridges.

Keywords *High damping rubber, nonlinear viscosity law, finite element implementation, isolation bearing, expansion joints.*

Introduction

General

Use of laminated rubber bearings for seismic isolation is widely recognized in reducing earthquake induced damages (Kelly 1997). Vulcanized natural rubber or high damping rubber is commonly used with alternate layers of steel plates (Fig 1c) for fabricating such bearings. The steel plates placed in horizontal layers provide large vertical stiffness for resisting superimposed dead load but at the same time ensure the low horizontal shear stiffness of the device. The horizontal flexibility offered thus by the device is important in resisting lateral loads due to earthquakes. In addition, steel plate laminated rubber expansion joints (Fig. 2 and 3) are often used at central hinge locations of balanced cantilever bridges (c.f. Spuler et al. 2010). In such arrangements, the expansion joints generally used to accommodate temperature induced bridge seating displacements also transfer vertical reaction forces arising from the moving loads to the adjacent spans in service conditions. Two approaches are followed in the industry to design and shape these devices. The first approach relies on data obtained from testing

the prototype devices whereas the other approach follows a rigorous numerical procedure e.g. finite element (FE) method that considers geometric and material nonlinearities. Both approaches have their own deficiencies; however the later one offers a better flexibility in making design iterations. Thus, sophistication in development and implementation of an adequate material law describing the pertinent mechanical behaviors of rubber-like materials is crucial.

Rate-dependent behavior in rubber

Mechanical responses of rubbers depend strongly on the past loading history, current strain and the strain rate (c.f. Amin et al. 2006a; Bergström and Boyce 1998; Lion 1996; Miehe and Keck 2000; for state-of-the-art reviews). In high damping rubber, these dependences are strongly nonlinear (Amin 2001). The monotonic rate-independent response of rubber-like materials is generally reproduced by rate-independent hyperelasticity models (c.f. Mooney 1940; Rivlin and Saunder 1951; Treloar 1944). A detailed review of the historical development of different hyperelasticity models is presented elsewhere (Amin et al. 2002; Shariff 2000). In order to represent the viscosity induced strain-rate effect, the total stress is usually decomposed into equilibrium response and overstress response. The total strain is decomposed into elastic and inelastic strains (c.f. Fig 4 for Zener Model) through multiplicative decomposition of the strain tensor (Lubliner 1973, 1985). The viscosity effect is reproduced by a relation between the overstress and the inelastic strain rate (Huber and Tsakmakis 2000). The equilibrium and instantaneous responses of the material are defined as the boundary state responses obtained from a specimen at infinitely slow and fast rates, respectively. These two extreme responses define the boundary of a domain in which viscosity effects comes into play. Multi-step relaxation (MSR) tests and monotonic tests at fast rates are recognized as the standard tests to characterize these elastic boundary states. Simple relaxation (SR) tests are used to characterize the viscosity phenomena that exist in between the two boundary states (c.f. Amin et al. 2002; Huber and Tsakmakis 2000). The difference between the current stress and the equilibrium stress is known as the overstress. Haupt and Sedlan (2001) assumed a nonlinear dependence of the viscosity on the current strain while Amin et al. (2006a) proposed a general relation between the

overstress and the inelastic strain rate of both natural and high damping rubber. Experimental evidences reported there have shown the strong dependence of the relation on past maximum overstress and current strain. The adequacy of the model in reproducing MSR, SR and monotonic tests in compression and shear regimes was verified with experimental observations. Furthermore, the model was also successful in reproducing an independent set of test results at simple shear and uniaxial compression regimes with a unique set of parameters. More recently, Bhuiyan et al. (2009) identified the similar effect in high damping rubber bearings and provided a thorough rheological characterization.

Numerical treatment of rate-dependent phenomena

The experimental identification and subsequent characterization of the phenomena are recognized to be the primary steps in developing a rational constitutive model and to evaluate the parameters.

However, the realization of benefits from such advancements for the design depends on successful implementation of the model in a FE procedure. In such procedure, the nonlinear equations are solved in linearized form to ascertain the stress field within the device (c.f. Simo et al. 1985; Simo 1987; Simo and Taylor 1991) by solving a boundary-value problem. Amin et al. (2006b) provided a state-of-the-art review on the FE analysis of rubber devices. As the primary step, they also implemented an improved hyperelasticity model into FEAP, which is a general purpose open source finite element software (Taylor 2006) partially documented in Zienkiewicz and Taylor (2006). The capability of the improved hyperelasticity model in simulating rate-independent responses, e.g. equilibrium and elastic responses were tested there by comparing experimental results in compression and shear regimes. Hasanpour and Ziaei-Rad (2008) presented a visco-hyperelasticity model and the computational strategy for

simulating the rate-dependent response of polymers at large strains. The model was adequate in reproducing the equilibrium and instantaneous responses but completely failed to represent the stress relaxation phenomenon. Nevertheless, simulation of relaxation phenomenon is one of the major attainable benchmarks in assessing the worthiness of a viscoelasticity model. Hasanpour et al. (2009) further states, in a later communication about the difficulty in making analytical calculation of the tangent modulus, which is an essential step in the Newton's method. Dal and Kaliske (2009) presented a thorough numerical treatment to implement the Bergström and Boyce viscoelasticity model (Bergström and Boyce 1998) in a FE code. However, the model having a micromechanics based inspiration was found by the authors not to be applicable for general rate-dependent cases e.g. simulation of devices using high damping rubber. On the other hand, the fundamental promise demonstrated by the visco-hyperelasticity model (Amin et al. 2006a) in analytical cases on describing the viscosity effect in high damping rubber and natural rubber is yet to be explored in detail for solving boundary value problems in a FE technique. Nevertheless, the classical measurements presented there still motivate the current researchers in developing and implementing new models (Johlitz et al. 2007, 2008; Spathis and Kontou 2008).

Objectives and methodology

The potentials of the visco-elasticity model proposed in Amin et al. (2006a) motivated the authors to outline a computational strategy for finite element analysis of rubber bearings and expansion joints. In order to maintain simplicity, the scope of the current work was restricted towards simulation of one dimensional problem, in particular. The match of simulation results obtained using the proposed strategy on full-scale rubber bearings with the independent experiments are also checked. Finally, numerical experiments on rubber bearings of different shape factors and steel plate laminated

rubber expansion joints are conducted to indicate the applicability of the proposed method in a wider area.

Constitutive modeling

General framework

A 3- parameter Maxwell model (Zener Model) as shown in Fig 4 is used to model the rate-dependent behavior of rubber. The total stress is decomposed into two parts i.e. rate-independent equilibrium part and rate-dependent overstress part. To model the rate-dependency phenomenon, the hyperelastic models are required to be combined with rate-dependent model. In this work, the improved hyperelasticity model proposed by Amin et al. (2006b) has been used to combine with rate-dependent model (Huber Tsakmakis 2000) to determine the total stress-strain relation. Equation (1) represents the strain energy density function, W, expressed as a function of the invariants of deformation tensor of material considering as an incompressible and isotropic-elastic material.

$$W(I_1,I_2)=C_5(I_1-3)+\frac{C_3}{N+1}(I_1-3)^N+\frac{C_4}{M+1}(I_1-3)^M+C_2(I_2-3) \tag{1}$$

where, C_2, C_3, C_4, C_5, M and N are material parameters. The invariants of the left Cauchy-Green tensor can be written in terms of the principal stretches $\lambda_i (i=1,2,3)$,

$$I_1 = \mathrm{tr}\,\mathbf{B} = \lambda_1^2+\lambda_2^2+\lambda_3^2$$

$$I_2 = \frac{1}{2}\left\{(\mathrm{tr}\mathbf{B})^2 - \mathrm{tr}(\mathbf{BB})\right\} = (\lambda_1\lambda_2)^2+(\lambda_2\lambda_3)^2+(\lambda_3\lambda_1)^2$$

From Truesdell and Noll (2004), the Cauchy stress $\mathbf{T}$ can be expressed as

$$\mathbf{T} = -p\mathbf{1} + \mathbf{T}_E \tag{2}$$

$$\mathbf{T}_E = 2\frac{\partial W}{\partial I_1}\mathbf{B} - 2\frac{\partial W}{\partial I_2}\mathbf{B}^{-1} \tag{3}$$

where $\mathbf{1}$ is the identity tensor, p is the Lagrange multiplier that can be determined from the boundary condition and the subscript ' E ' defines the extra stress.

From the model structures shown in Fig 4, the extra stress tensor can be written as the sum of the equilibrium part $\mathbf{T}_E^{(E)}$ and the overstress part $\mathbf{T}_E^{(OE)}$:

$$\mathbf{T}_E = \mathbf{T}_E^{(E)} + \mathbf{T}_E^{(OE)} \tag{4}$$

with

$$\mathbf{T}_E^{(E)} = 2\frac{\partial W^{(E)}}{\partial I_{1\mathbf{B}}}\mathbf{B} - \frac{\partial W^{(E)}}{\partial I_{2\mathbf{B}}}\mathbf{B}^{-1} \tag{5}$$

$$\mathbf{T}_E^{(OE)} = 2\frac{\partial W^{(OE)}}{\partial I_{1\mathbf{B}_e}}\mathbf{B}_e - \frac{\partial W^{(OE)}}{\partial I_{2\mathbf{B}_e}}\mathbf{B}_e^{-1} \tag{6}$$

where $\mathbf{B} = \mathbf{F}\mathbf{F}^T$, $\mathbf{B}_e = \mathbf{F}_e\mathbf{F}_e^T$ and $\mathbf{I}_{1B}$ and $\mathbf{I}_{2B}$ are the first and second invariants of the left Cauchy-Green tensor $\mathbf{B}$. The subscript ' e ' denotes the quantities related to $\mathbf{F}_e$.

Following the concept of Huber and Tsakmakis (2000), the rate of left Cauchy-Green deformation tensor can be expressed as

$$\dot{\mathbf{B}}_e = \mathbf{B}_e\mathbf{L}^T + \mathbf{L}\mathbf{B}_e - \frac{2}{\eta}\mathbf{B}_e\left(\hat{\mathbf{P}}_E - \hat{\mathbf{P}}_E^{(E)}\right) \tag{7}$$

The superimposed dot indicates the material time derivative, η is the viscosity function, $\mathbf{P}_E$ is Mandel stress tensor and $\mathbf{L}$ is the velocity gradient expressed as,

$$\mathbf{L} = \dot{\mathbf{F}}\mathbf{F}^{-1} \tag{8}$$

Evolution of nonlinear viscosity

Amin et al. (2006a) followed the general constitutive theory based on Huber and Tsakmakis (2000) to propose an explicit description of the evolution equation of nonlinear viscosity by analyzing the experimental data in compression and shear. Equation (9) represents the constitutive equation of viscosity of the power law type (Amin et al. 2006a) in general three dimensional form:

$$\hat{\mathbf{D}}_i = \frac{\left\|\hat{\mathbf{P}}_{\mathrm{E}}^{(\mathrm{OE})}\right\|^{\delta}}{\eta_0 \pi^{\delta} \left\|\mathbf{B}\right\|^{\varphi}} . \hat{\mathbf{P}}_{\mathrm{E}}^{(\mathrm{OE})} \tag{9}$$

where φ, δ and η_0 are material parameters to be determined and $\|\boldsymbol{\omega}\| = \sqrt{\boldsymbol{\omega}.\boldsymbol{\omega}}$ is the magnitude of a tensor. The closed form of the evolution equation of the constitutive equation of nonlinear viscosity can be obtained from Equation (9).

$$\frac{1}{\eta\left(\hat{\mathbf{P}}_{\mathrm{E}}^{(\mathrm{OE})}, \mathbf{B}\right)} = \frac{1}{\eta_0}\left(\frac{\left\|\hat{\mathbf{P}}_{\mathrm{E}}^{(\mathrm{OE})}\right\|}{\pi}\right)^{\delta} \left\|\mathbf{B}\right\|^{-\varphi} \tag{10}$$

In Equation (9) and (10), the constant $\pi = (1\,\mathrm{MPa})$ has been introduced for dimensional reasons.

Computational strategy for viscosity effect

In analyzing the rubber bearings and expansion joints, uniaxial compression and simple shear are the relevant deformation modes to consider. The first order differential equation presented in Equation (7) and (10) for nonlinear evolution of viscosity is

decomposed into one dimensional form in next two subsections. A standard numerical method is applied to solve the one dimensional rate equations. The approach is novel for its inherent simplicity but possesses a limitation in solving a problem for arbitrary or unknown deformation modes (Bhuiyan et al. 2007; Hossain 2007).

Uniaxial compression loading: Assuming rubber as incompressible material, the total deformation gradient tensor can be written as

$$\mathbf{F} = \begin{bmatrix} \lambda & 0 & 0 \\ 0 & \dfrac{1}{\sqrt{\lambda}} & 0 \\ 0 & 0 & \dfrac{1}{\sqrt{\lambda}} \end{bmatrix} \tag{11}$$

Thus the left Cauchy-Green strain deformation tensor can be evaluated as

$$\mathbf{B} = \mathbf{F}\mathbf{F}^{\mathrm{T}} = \begin{bmatrix} \lambda^2 & 0 & 0 \\ 0 & \dfrac{1}{\lambda} & 0 \\ 0 & 0 & \dfrac{1}{\lambda} \end{bmatrix} \tag{12}$$

Similarly, for the intermediate spring as shown in Fig 4, one obtains

$$\mathbf{F}_{\mathrm{e}} = \begin{bmatrix} \lambda_e & 0 & 0 \\ 0 & \dfrac{1}{\sqrt{\lambda_e}} & 0 \\ 0 & 0 & \dfrac{1}{\sqrt{\lambda_e}} \end{bmatrix} \text{ and } \mathbf{B}_e = \mathbf{F}_{\mathrm{e}}\mathbf{F}_{\mathrm{e}}^{\mathrm{T}} = \begin{bmatrix} \lambda_e^2 & 0 & 0 \\ 0 & \dfrac{1}{\lambda_e} & 0 \\ 0 & 0 & \dfrac{1}{\lambda_e} \end{bmatrix} \tag{13}$$

The rate of deformation gradient tensors are given as

$$\mathbf{L}=\dot{\mathbf{F}}\mathbf{F}^{-1}=\dot{\lambda}\begin{bmatrix}\frac{1}{\lambda} & 0 & 0\\ 0 & -\frac{1}{2\lambda} & 0\\ 0 & 0 & -\frac{1}{2\lambda}\end{bmatrix} \quad \text{and} \quad \dot{\mathbf{B}}_e=\dot{\lambda}_e\begin{bmatrix}2\lambda_e & 0 & 0\\ 0 & -\frac{1}{\lambda_e^2} & 0\\ 0 & 0 & -\frac{1}{\lambda_e^2}\end{bmatrix} \tag{14}$$

From Equation (7), it yields

$$\mathbf{B}_e\mathbf{L}^{\mathrm{T}}=\mathbf{B}_e\mathbf{L}=\dot{\lambda}\begin{bmatrix}\frac{\lambda_e^2}{\lambda} & 0 & 0\\ 0 & -\frac{1}{2\lambda\lambda_e} & 0\\ 0 & 0 & -\frac{1}{2\lambda\lambda_e}\end{bmatrix} \quad \text{and} \quad \left(\mathbf{T}-\mathbf{T}^{(E)}\right)^D=\begin{bmatrix}\mathrm{T}_{11}^{(\mathrm{OE})} & 0 & 0\\ 0 & \mathrm{T}_{22}^{(\mathrm{OE})} & 0\\ 0 & 0 & \mathrm{T}_{33}^{(\mathrm{OE})}\end{bmatrix}^D \tag{15}$$

Now, substituting the Equations (14) and (15) into Equation (7) yields

$$\begin{aligned}\dot{\lambda}_e\begin{bmatrix}2\lambda_e & 0 & 0\\ 0 & -\frac{1}{\lambda_e^2} & 0\\ 0 & 0 & -\frac{1}{\lambda_e^2}\end{bmatrix}&=\dot{\lambda}\begin{bmatrix}\frac{\lambda_e^2}{\lambda} & 0 & 0\\ 0 & -\frac{1}{2\lambda\lambda_e} & 0\\ 0 & 0 & -\frac{1}{2\lambda\lambda_e}\end{bmatrix}\\ +\dot{\lambda}\begin{bmatrix}\frac{\lambda_e^2}{\lambda} & 0 & 0\\ 0 & -\frac{1}{2\lambda\lambda_e} & 0\\ 0 & 0 & -\frac{1}{2\lambda\lambda_e}\end{bmatrix}&-\frac{2}{\eta_0}\left(\frac{\left\|\mathbf{T}^{(\mathrm{OE})}\right\|}{\pi}\right)^{\delta}\|\mathbf{B}\|^{-\varphi}\begin{bmatrix}\lambda_e^2 & 0 & 0\\ 0 & \frac{1}{\lambda_e} & 0\\ 0 & 0 & \frac{1}{\lambda_e}\end{bmatrix}\begin{bmatrix}\mathbf{T}_{11}^{(\mathrm{OE})} & 0 & 0\\ 0 & \mathbf{T}_{11}^{(\mathrm{OE})} & 0\\ 0 & 0 & \mathbf{T}_{11}^{(\mathrm{OE})}\end{bmatrix}^D\end{aligned} \tag{16}$$

Considering the first normal term which corresponds to the loading condition and viscosity at each strain level constant, we isolate the relevant rate equation

$$2\dot{\lambda}_e\lambda_e=2\frac{\dot{\lambda}}{\lambda}\lambda_e^2-\frac{4}{3}\mathrm{T}_{11}^{(\mathrm{OE})}\lambda_e^2\frac{1}{\eta_0}\left(\frac{\left|\mathrm{T}^{(\mathrm{OE})}\right|}{\pi}\right)^{\delta}|\lambda|^{-2\varphi} \tag{17}$$

$$\dot{\lambda}_e=2\frac{\dot{\lambda}}{\lambda}\lambda_e-\frac{2}{3}\mathrm{T}_{11}^{(\mathrm{OE})}\lambda_e\frac{1}{\eta_0}\left(\frac{\left|\mathrm{T}^{(\mathrm{OE})}\right|}{\pi}\right)^{\delta}|\lambda|^{-2\varphi} \tag{18}$$

Equation (18) is solved by a standard numerical method with adequate solution steps.

Simple shear loading: The total deformation gradient and the left Cauchy-Green tensor are given by the following expressions:

$$\mathbf{F} = \begin{bmatrix} 1 & \gamma & 0 \\ 0 & 1 & 0 \\ 0 & 0 & 1 \end{bmatrix} \text{ and } \mathbf{B} = \mathbf{F}\mathbf{F}^{\mathrm{T}} = \begin{bmatrix} 1+\gamma^2 & \gamma & 0 \\ \gamma & 1 & 0 \\ 0 & 0 & 1 \end{bmatrix} \tag{19}$$

Similarly, for intermediate spring, these two quantities can be written as

$$\mathbf{F}_{\mathrm{e}} = \begin{bmatrix} 1 & \gamma_e & 0 \\ 0 & 1 & 0 \\ 0 & 0 & 1 \end{bmatrix} \text{ and } \mathbf{B}_{\mathrm{e}} = \mathbf{F}_{\mathrm{e}}\mathbf{F}_{\mathrm{e}}^{\mathrm{T}} = \begin{bmatrix} 1+\gamma_e^2 & \gamma_e & 0 \\ \gamma_e & 1 & 0 \\ 0 & 0 & 1 \end{bmatrix} \tag{20}$$

The velocity gradient and the rate of the elastic left Cauchy-Green tensor read as

$$\mathbf{L} = \dot{\mathbf{F}}\mathbf{F}^{-1} = \begin{bmatrix} 0 & \dot{\gamma} & 0 \\ 0 & 0 & 0 \\ 0 & 0 & 0 \end{bmatrix} \text{ and } \dot{\mathbf{B}}_e = \begin{bmatrix} 2\gamma_e\dot{\gamma}_e & \dot{\gamma}_e & 0 \\ \dot{\gamma}_e & 0 & 0 \\ 0 & 0 & 0 \end{bmatrix} \tag{21}$$

Using Equation (17), Equation (6) yields

$$\mathbf{B}_{\mathrm{e}}\mathbf{L}^{\mathrm{T}} = \begin{bmatrix} \gamma_e\dot{\gamma} & 0 & 0 \\ \dot{\gamma} & 0 & 0 \\ 0 & 0 & 0 \end{bmatrix} \text{ and } \mathbf{L}\mathbf{B}_{\mathrm{e}}^{\mathrm{T}} = \begin{bmatrix} \gamma_e\dot{\gamma} & \dot{\gamma} & 0 \\ 0 & 0 & 0 \\ 0 & 0 & 0 \end{bmatrix} \tag{22}$$

$$\left(\mathbf{T}-\mathbf{T}^{(E)}\right)^D = \begin{bmatrix} \mathrm{T}_{11}^{(\mathrm{OE})} & \mathrm{T}_{12}^{(\mathrm{OE})} & 0 \\ \mathrm{T}_{21}^{(\mathrm{OE})} & \mathrm{T}_{22}^{(\mathrm{OE})} & 0 \\ 0 & 0 & \mathrm{T}_{33}^{(\mathrm{OE})} \end{bmatrix}^D \tag{23}$$

Now, substituting the Equations (21) and (22) into Equation (7) yields

$$\begin{bmatrix} 2\gamma_e\dot{\gamma}_e & \dot{\gamma}_e & 0 \\ \dot{\gamma}_e & 0 & 0 \\ 0 & 0 & 0 \end{bmatrix} = \begin{bmatrix} \gamma_e\dot{\gamma} & 0 & 0 \\ \dot{\gamma} & 0 & 0 \\ 0 & 0 & 0 \end{bmatrix} + \begin{bmatrix} \gamma_e\dot{\gamma} & \dot{\gamma} & 0 \\ 0 & 0 & 0 \\ 0 & 0 & 0 \end{bmatrix} - \frac{2}{\eta_0}\left(\frac{\left\|\mathbf{T}^{(OE)}\right\|}{\pi}\right)^{\delta}\|\mathbf{B}\|^{-\phi}$$
$$\begin{bmatrix} 1+\gamma_e^2 & \gamma_e & 0 \\ \gamma_e & 1 & 0 \\ 0 & 0 & 1 \end{bmatrix}\begin{bmatrix} T_{11}^{(OE)} & T_{12}^{(OE)} & 0 \\ T_{21}^{(OE)} & T_{22}^{(OE)} & 0 \\ 0 & 0 & T_{33}^{(OE)} \end{bmatrix}^{D} \qquad (24)$$

Considering the off-diagonal terms which correspond to the simple shear loading condition, we isolate the relevant rate equation

$$\dot{\gamma}_e = \dot{\gamma} - \frac{4}{3}\frac{\gamma_e}{\eta_0}T_{12}^{(OE)}\left(\frac{\left|P_{12}^{(OE)}\right|}{\pi}\right)^{\delta}|\gamma|^{-2\phi} \qquad (25)$$

In this context, the authors are aware of ignoring the effect of normal components of Equation (24) for avoiding the complexity. The simplification conforms also with the experimental conditions e.g. simple shear. Equation (25) is solved by a standard numerical method with adequate solution steps.

Material parameters

Equation (1) contains the material parameters $C_2, C_3, C_4, C_5, M \text{ and } N$ to represent the strain energy density function for the elasticity response; Equation (10) includes the constants $\varphi, \delta \text{ and } \eta_0$, which belong to the nonlinear viscosity function. Tables 1 and 2 present the numerical values of the material parameters for high damping rubber. In order to identify the parameters ($C_2, C_3, C_4, C_5, M \text{ and } N$) of the hyperelasticity model (Eq. 1), the experimental data obtained in compression and shear regime were used along with a scheme involving the least-square method to minimize the residuals (Amin et al. 2006b). The viscosity parameters were determined by applying the least-square method on $\hat{\mathbf{D}}_i$ vs. $\hat{\mathbf{P}}_E^{(OE)} \Big/ \hat{P}_E^{(OE)}\Big|_{max}$ relation and $\|\mathbf{B}\|$ vs. $\hat{P}_E^{(OE)}\Big|_{max}$ relation so that Equation (9) is satisfied; where $\hat{P}_E^{(OE)}\Big|_{max}$ is the past maximum overstress that existed just at the very beginning of the relaxation process and $\|\mathbf{B}\|$ is magnitude the current deformation.

For details, please refer to Amin et al. (2006a).

Model verification

The solution strategy to compute the evolution equation (7) as described in earlier section is incorporated in a versatile finite element program, FEAP (Taylor 2006). Three-dimensional (3D) finite element analysis is carried out using the FE models of the specimens as shown in Fig 1a and 1b for compression and simple shear, respectively. Simulation results are checked with experiments to verify the numerical accuracy. In order to check the effect of the mesh size on the results a mesh sensitivity analysis was carried out. 3D models were also reduced to two dimensions (2D) for comparison. Eight-node brick element is used to model the rubber and steel. Both the geometric and material nonlinearities of rubber layers are considered in the analysis. Steel is considered to be linearly elastic.

Mesh sensitivity

The convergence of the FE mesh with smaller mesh size is verified in Fig 5. The comparison of responses in Fig 5a for uniaxial compression show the inadequacy of a 2D mesh in simulation whereas a 3D mesh with 24 elements were found to be reasonable. In Fig 5b, the simple shear case is presented. A 2D coarse mesh with a number of 24 elements in one direction was found to be sufficient for the tested shape factor. Mesh sensitivity test was conducted on a single layer rubber sheet having shape factor 12 and the dimensions given in Table 3 and Fig 5. Here shape factor is defined as:

$$\text{Shape factor} = l_a l_b \Big/ 2t_r\left(l_a + l_b\right) \tag{26}$$

where $l_a l_b$ is the loaded area of the bearing and $2t_r\left(l_a + l_b\right)$ is the load free area of the bearing (Fig 1).

Verification with experiments

The adequacy of the proposed computational strategy and the FE code hence prepared are verified by comparing simulation results obtained using converged mesh size and the results from SR tests. In SR test, a rubber specimen is maintained a desired level of strain at a constant strain rate and the stress required to maintain this strain is measured for the requisite period of time (relaxation time). The maximum stress occurs when the deformation takes place, and the stress decreases gradually with time from the maximum value. The stretch rate of 0.5/s followed by a relaxation time of 10 min with a stretch level of 0.5 was used in uniaxial compression mode of SR tests; however, the shear strain rate of 0.5/s was followed by 10 mins with a constant strain level of 2.50 for the mode of simple shear in SR tests (c.f. Amin et al. 2002; Amin et al. 2006a).

Fig 6a presents the comparison in uniaxial compression and Fig 6b the same for simple shear case. A series of monotonic compression tests at different constant stretch rates up to 0.5 stretch level were carried out. The constant stretch-rate cases within the range of 0.001–0.96/ s were considered in the test. The simple shear tests were carried out in the similar fashion of the uniaxial compression tests; however, the shear strain rates were within the range of 0.05/s -0.5/s and the shear strain was increased to 2.50 (c.f. Amin et al. 2002; Amin et al. 2006a). The agreement between the experiment and the simulation during the long-term stress relaxation is excellent. The simulation performance in between the instantaneous and equilibrium states, more definitely in first 20 seconds of SR history as presented here seems to be distinctly improved that compared to that presented in Hasanpour and Ziaei-Rad (2008) for their data. The simulation of monotonic compression and simple shear experiments are compared with experiments in Fig 7. The correlation between the simulation and experimental results are well apparent for the investigated strain-rate cases. At a slower strain rate the simulation results have a better conformity with those of the experiments but at faster strain rate it does not agree so well. Fig 8 presents the stress contour for the two deformation cases. The homogeneous deformation both in uniaxial compression and simple shear modes are obtained from simulation. The observation conforms directly to the experimental boundary condition.

Finally, the simulation of the shear stress-strain response obtained from a prototype bearing with a shape factor of 12 is compared with the experiments in Fig 9. The comparison is independent of its kind as long as the test data points presented in Figure 9 were not used for parameter identification (Tables 1 and 2). Nevertheless, an excellent correlation between the simulation and the experiments is clearly visible. The respective contours for displacement and shear stress are presented in Fig 10. The contours are reasonably converging and informative as well in indicating the regions where large displacement and stress concentration take place.

Numerical experiments

The verification results presented in preceding sections offer reasonable confidence in making numerical experiments within the scope of the proposed strategy. In this context, this section provides information about the shape factor effect of bearing on stress field in a steel plate laminated rubber expansion joint.

Shape factor effect in laminated rubber bearings

Fig 11 presents the shear responses of the bearing obtained from bearings with different shape factors (Table 3). The trend of increase in response for the bearings of large shape factor is noticeable in the figure. At large shape factors, the shear stiffness of the bearing increases at a non-proportional rate. Furthermore, in addition to the nonlinearity in the response at low, moderate and large strain levels depicted by the hyperelasticity relation (Equation 1), the influence of the viscosity on the response of the system is also perceivable. All this information supplements the works of Imbimbo and Luca (1998) for uniaxial compression and Matsuda (2004) for shear deformation.

Steel plate laminated rubber expansion joints

Figs 2 and 3 presented the as-built basic geometry of a steel plate laminated rubber expansion joint used in a bridge of Bangladesh. Replacement of such joints on the bridge deck needs closure of the bridge and considered therefore as a major repair work. Separation of bottom layers of rubber from steel plate is found to initiate the damage of

the joints. Fig 12 presents the indicative interfacial stress field of such a typical expansion joint obtained using the simulation results. The high stress concentration regions located around the steel plate boundaries are shown as stress contours. 3D Solid elements are used to model the rubber and steel layers. A loading configuration combined with compression and shear loadings is used in the FE simulation. However, to remain in line with the leading objective of this essay, the authors avoided further complexities associated with truly understanding and modeling the interface phenomenon between rubber and steel in details. Instead, an absolute bonding between rubber and steel plate was assumed. Such simplification may weaken the precise assessment of stresses in stress concentration zones due to ignoring additional effects in the FE model, e.g. frictional slip, shear, adhesion, elastic mismatch etc. that may act in those zones. Yet, the resulting qualitative high stress concentration regions located around the interface of rubber and steel layers as obtained from the performed simulation closely conforms to the line of failures observed in the field.

Conclusion

A constitutive model of visco-hyperelasticity for rubber has been implemented into a computational strategy to solve boundary value problems under compression and simple shear. The development avoids rigorous mathematical manipulations, therefore seems suitable for use as a design aid. However, additional attempts are made in the work to assure the readers about the adequacy of such simplification in reproducing experimental results from rubber specimens and rubber bearings for the relevant deformation modes. The developed code has been used to conduct numerical experiments on rubber bearings of different shape factors and rubber expansion joints. The information obtained to this effect conform to other published results and therefore, also useful at the design desk.

Acknowledgements

The authors are very grateful to Professor H. Horii, Department of Civil Engineering, University of Tokyo, Japan for his valuable comments and suggestions and particularly for allowing us to use the experimental facilities of his laboratory to carry out the mechanical tests in the investigation. The authors gratefully acknowledge the kind cooperation extended by the Yokohama Rubber Co. by providing test specimens. The authors also sincerely appreciate the funding provided by the Japanese Ministry of Education, Science, Sports and Culture as Grant-in-Aid for Scientific Research (C) (No. 12650457) to carryout this research.

References

Amin, A.F.M.S. (2001). "Constitutive Modeling for Strain-rate Dependency of Natural and High Damping Rubbers." Doctoral Dissertation, Saitama University, Japan.

Amin, A.F.M.S., Alam, M.S. and Okui, Y. (2002). "An improved hyperelasticity relation in modeling viscoelasticity response of natural and high damping rubbers in compression: experiments, parameter identification and numerical verification."*Mech. Mater*. 34, 75-95.

Amin, A.F.M.S., Lion, A., Sekita, S., Okui, Y. (2006a). "Nonlinear dependence of viscosity in modeling the rate-dependent response of natural and high damping rubbers in compression and shear: Experimental identification and numerical verification." *Int. J. Plasticity.*, 22 (9), 1610-1657.

Amin, A.F.M.S., Wiraguna, S.I., Bhuiyan, A.R., Okui, Y. (2006b). "Hyperelasticity model for FE analysis of natural and high damping rubbers in compression and shear." *ASCE J. Eng. Mech*., 132(1), 54-64.

Bergström, J.S. and Boyce, M. C. (1998). "Constitutive modeling of the large strain time-dependent behavior of elastomers." *J. Mech. Phys. Solids*., 46, 931-954.

Bhuiyan, A.R., Amin, A.F.M.S., Hossain, T., Okui, Y. (2007). "Nonlinear viscosity law for rate-dependent response of high damping rubber: FE implementation and verification." *Proceedings of 5th European Conference for Constitutive Models for Rubber*, Boukamel, Laiarinandrasana, Meo, Verron (eds), Taylor & Francis Group, London, ISBN 978-0-415-45442-1, 274-284.

Bhuiyan, A.R., Okui, Y., Mitamura, H. and Imai, T. (2009). "A rheology model of high damping rubber bearings for seismic analysis: Identification of nonlinear viscosity." *Int. J. Solids Struct.*, 46, 1778-1792.

Dal, H. and Kaliske, M. (2009). "Bergström-Boyce model for nonlinear finite rubber viscoelasticity: theoretical aspects and algorithmic treatment for the FE method." *Comput. Mech.*, 44(6), 809-823.

Hasanpour, K. and Ziaei-Rad, S. (2008)."Finite element simulation of polymer behaviour using a three-dimensional, finite deformation constitutive model." *Comp. Struct.* , 86, 1643-1655.

Hasanpour, K., Ziaei-Rad, S., Mahzoon, M. (2009). "A large deformation framework for compressible viscoelastic materials: Constitutive equations and finite element implementation." *Int. J. Plasticity*, 25, 1154–1176.

Haupt, P. and Sedlan, K. (2001). "Viscoplasticity of elastomeric materials: experimental facts and constitutive modeling." *Arch. Appl. Mech.*, 71, 89-109.

Hossain, T. (2007). "Finite Element Formulation and Modelling of Rate Dependent Response of Natural and High Damping Rubbers." M.Sc. Engg. Thesis, Department of Civil Engineering, Bangladesh University of Engineering and Technology, Dhaka, Bangladesh

Huber, N. and Tsakmakis, C. (2000). "Finite deformation viscoelasticity laws." *Mech. Mater*., 32, 1-18.

Imbimbo, M. and Luca, A.D. (1998). "F.E. stress analysis of rubber bearings under axial loads." *Comp. Struct.* 68, 31-39.

Johlitz, M., Diebels, S., Batal, J., Steeb, H. and Possart, W. (2008). "Size effects in polyurethane bonds: experiments, modelling and parameter identification." *J. Mater. Sci.*, 43, 4768-4779.

Johlitz, M., Steeb, H., Diebels, S., Chatzouridou, A., Batal, J. and Possart, W. (2007). "Experimental and theoretical investigation of nonlinear viscoelastic polyurethane systems." *J. Mater. Sci.*, 42, 9894-9904.

Kelly, J.M. (1997). *Earthquake Resistant Design with Rubber*, Springer-Verlag, London.

Lion, A. (1996). "A constitutive model for carbon black filled rubber: experimental investigations and mathematical representation." *Continuum Mech. Thermodyn.,* 8, 153-169.

Lubliner, J. (1985). "A model for rubber viscoelasticity." *Mech. Res. Com.*, 12, 93-99.

Lubliner, J. (1973). "On the structure of the rate equations of materials with internal variables."*Acta Mecha.* 17, 109-119.

Matsuda, A. (2004). "Evaluation for Mechanical Properties of Laminated Rubber Bearings Using Finite Element Analysis." *J. Press. Vess. Tech.*, 126, 134-140.

Miehe, C. and Keck, J. (2000). "Superimposed finite elastic-viscoelastic-plastoelastic stress response with damage in filled rubbery polymers. Experiments, modeling and algorithmic implementation." *J. Mech. Phys. Solids.*, 48, 323-365.

Mooney, M. (1940). "A theory of large elastic deformation." *J. App. Phys.,* 11, 582-592.

Rivlin, R. S. and Saunders, D. W. (1951). "Large elastic deformations of isotropic materials VII. Experiments on the deformation of rubber." *Phil. Trans. R. Soc.*, 243, 251-288.

Shariff, M.H.B.M. (2000). "Strain energy function for filled and unfilled rubberlike material." *R. Chem. Tech.*, 73, 1-18.

Simo, J.C., Taylor, R.L. and Pister, K.S. (1985). "Variational and projection methods for the volume constraint in finite deformation elasto-palsticity." *Comput. Methods App. Mech. Eng.,* 51, 177-208.

Simo, J.C. (1987). "On a fully three dimensional finite strain viscoelastic damage model: Formulation and computational aspects." *Comput. Methods App. Mech. Eng.,* 60, 153-173.

Simo, J.C. and Taylor, R.L. (1991). "Quasi-incompressible finite elasticity in principal stretches. Continuum basis and numerical algorithms." *Comput. Methods App. Mech. Eng.*, 85, 273-310.

Spathis, G. and Kontou, E. (2008). "Modeling of nonlinear viscoelasticity at large deformations." *J. Mater. Sci.,* 43, 2046-2052

Spuler, T., Moor, G., Ghosh, C. (2010). "Supporting economical bridge construction – the central hinge bearings of the 2nd Shitalakshya Bridge." *Proceedings of IABSE-JSCE Joint Conference on Advances in Bridge Engineering-II,* Amin, Okui, Bhuiyan (eds.), ISBN: 978-984-33-1893-0, 275-280. International Association for Bridge and Structural Engineering, Zurich, Switzerland/Japan Society of Civil Engineers, Tokyo, 275–280.

Taylor, R.L. (2006). *FEAP- A finite element analysis program.* User manual, Version 8.1

Treloar, L.R.G. (1944). "Stress-strain data for vulcanized rubber under various types of deformations." *Trans. Fara. Soc.,* 40, 59-70.

Truesdell, C. and W. Noll. (2004). *The non-linear field theories of mechanics,* Springer-Verlag, Berlin.

Zienkiewicz, O.C., Taylor, R.L. (2006). The Finite Element Method for Solid and Structural Mechanics. 6th Ed., Butterworth-Heinemann, Oxford, U.K.

Table 1. Elasticity parameters

Responses	C_2 MPa	C_3 MPa	C_4 MPa	C_5 MPa	M	N
Equilibrium	0.145	1.182	-5.297	4.262	0.06	0.27
Instantaneous	0.166	2.477	-11.689	9.707	0.06	0.27
Overstress	0.021	1.295	-6.392	5.445		

Table 2. Viscosity parameters

η_0 (MPa)	δ	φ
1.63	1.46	2.29

Table 3. Geometry of Rubber Bearings with Different Shape Factors

Shape factor	a mm	B mm	t_s mm	t_r Mm	n_r	n_s
6	240	240	2	10	6	5
12	**240**	**240**	**2**	**5**	**6**	**5**
15	240	240	2	4	6	5
24	240	240	2	2.5	6	5
30	240	240	2	2	6	5

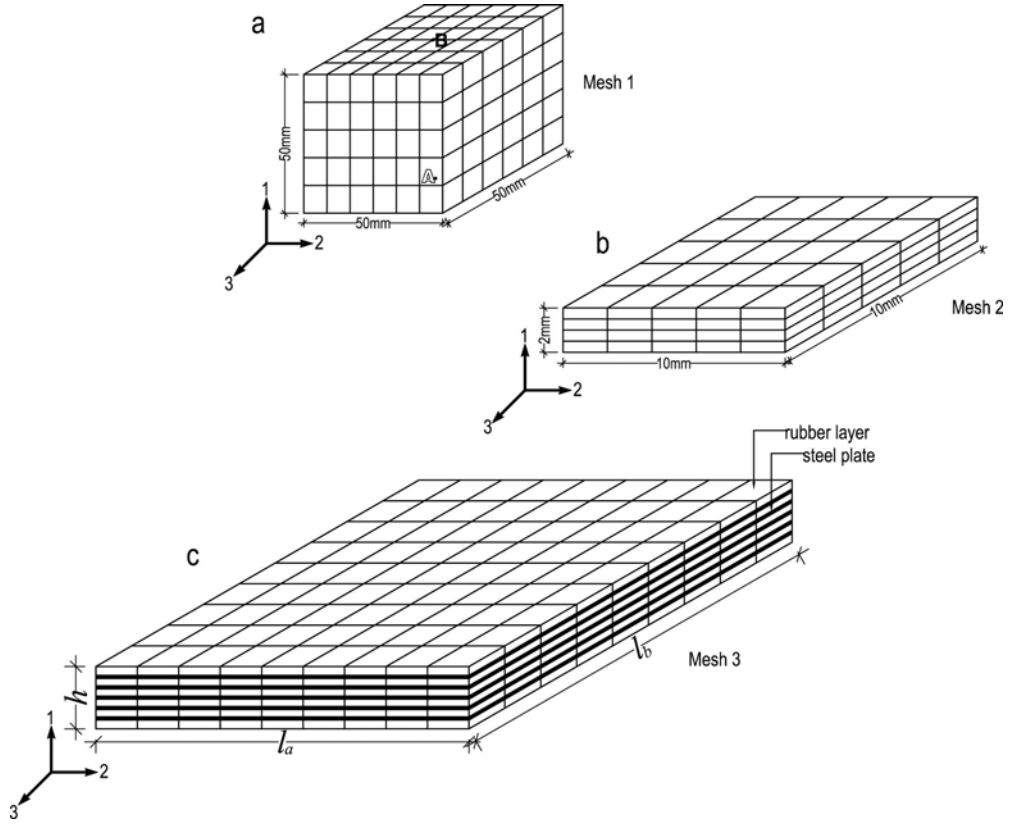

Figure 1. FE mesh used for numerical simulation. (a) Mesh 1: Uniaxial Compression. Boundary conditions: Node A at bottom surface (2-3 plane) is restrained in 1, 2 and 3-directions. All other nodes at bottom surface (2-3 plane) are free in 2, 3-directions and restrained in 1-direction. Node B at top edge is restrained in 2 and 3 directions. All other nodes at top edge are free. Displacement is applied along 1 direction. (b) Mesh 2: Simple shear. Boundary conditions: All nodes at the bottom edge (parallel to 2-3 plane) are restrained and fixed in 1, 2 and 3-directions All nodes at the top edge (parallel to 2-3 plane) are restrained in 1 and 3-directions. Displacement is applied along 2-direction. (c) Mesh 3: Rubber bearing. Boundary conditions: All nodes at the bottom edge (parallel to 2-3 plane) are restrained and fixed in 1, 2 and 3-directions. All nodes at the top edge (parallel to 2-3 plane) are restrained in 1 and 3-directions. Displacement is applied along 2-direction. Here, $h = n_r t_r + n_s t_s$. n_r: number of rubber layers; n_s: number of steel plates.

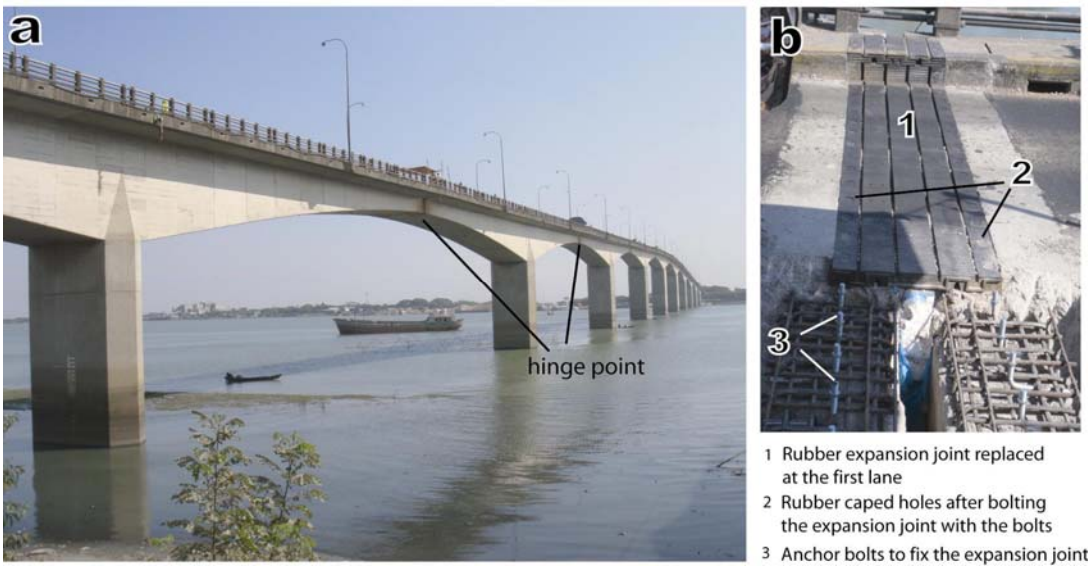

Figure 2. Replacement of rubber expansion joints of Japan-Bangladesh Friendship Bridge-I (23°31.858'N, 90°42.813'E) built in 1991 over the Meghna River, Bangladesh. (a) Hinge points depict the location of expansion joints. (b) Replacing the expansion joints as a part of bridge maintenance works.

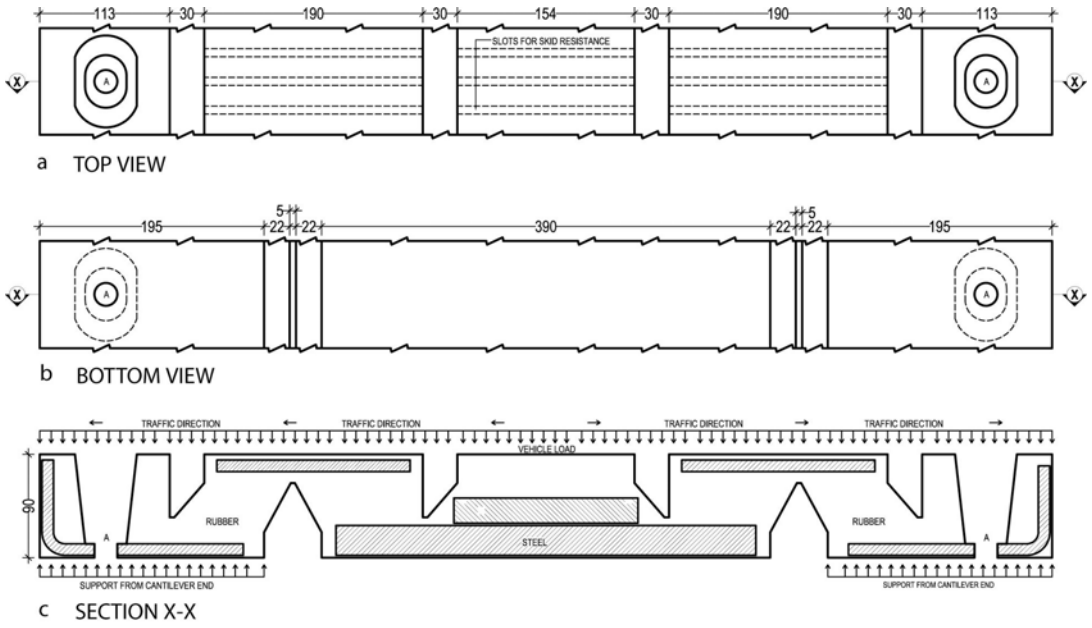

Figure 3. As-built geometric details of the expansion joint of Japan-Bangladesh Friendship Bridge-I (23°31.858'N, 90°42.813'E) over the Meghna River, Bangladesh (a) Top view, (b) Bottom view and (c) Longitudinal sectional view (Section X-X)

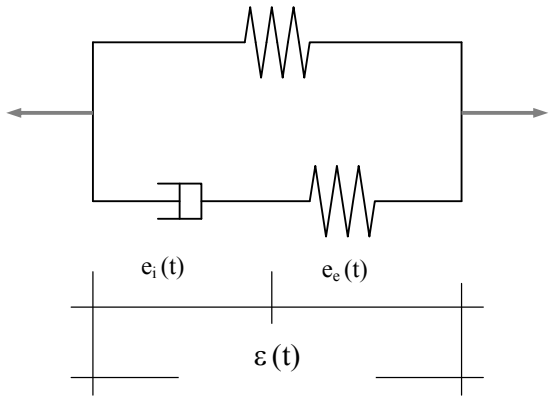

Figure 4. Zener model

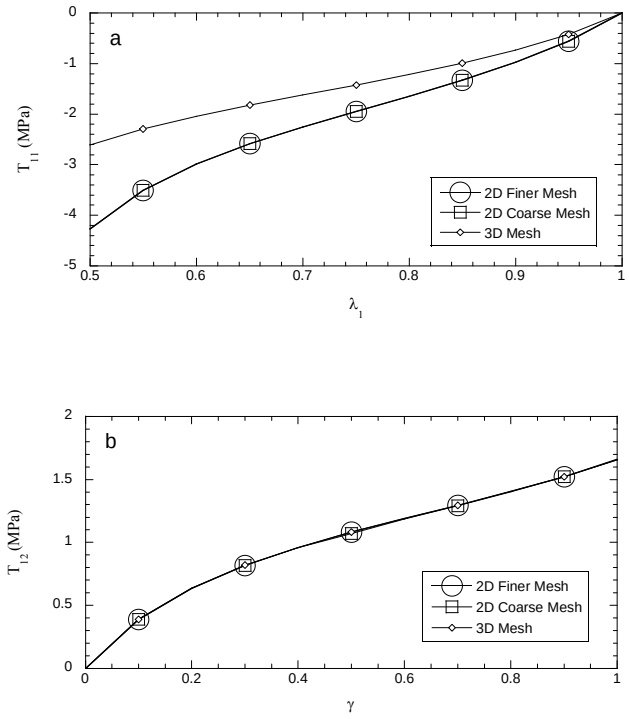

Figure 5. Effect of 1-direction mesh refinement on stress response in Mesh 3. (a) Effect on T_{11} stress; (b) Effect on T_{12} stress. 2D Coarse Mesh: A single rubber layer (l_a : $240mm$, $h(=t_r)$: $5mm$, shape factor 12, Table 3) is divided into 24 elements in 2-direction and 1 element in 1-direction. 2D Fine Mesh: A single rubber layer (l_a : $240mm$, $h(=t_r)$: $5mm$, shape factor 12, Table 3) is divided into 24 elements in 2-direction and 5 element in 1-direction. 3D Mesh: A single rubber layer (l_a : $240mm$, l_b : $240mm$, $h(=t_r)$: $5mm$, shape factor 12, Table 3) is divided into 24 elements in 2-direction and 3-direction and 1 element in 1-direction.

$$Shape\quad factor\quad =\quad l_a l_b \Big/ 2t_r\left(l_a\quad +\quad l_b\right)$$

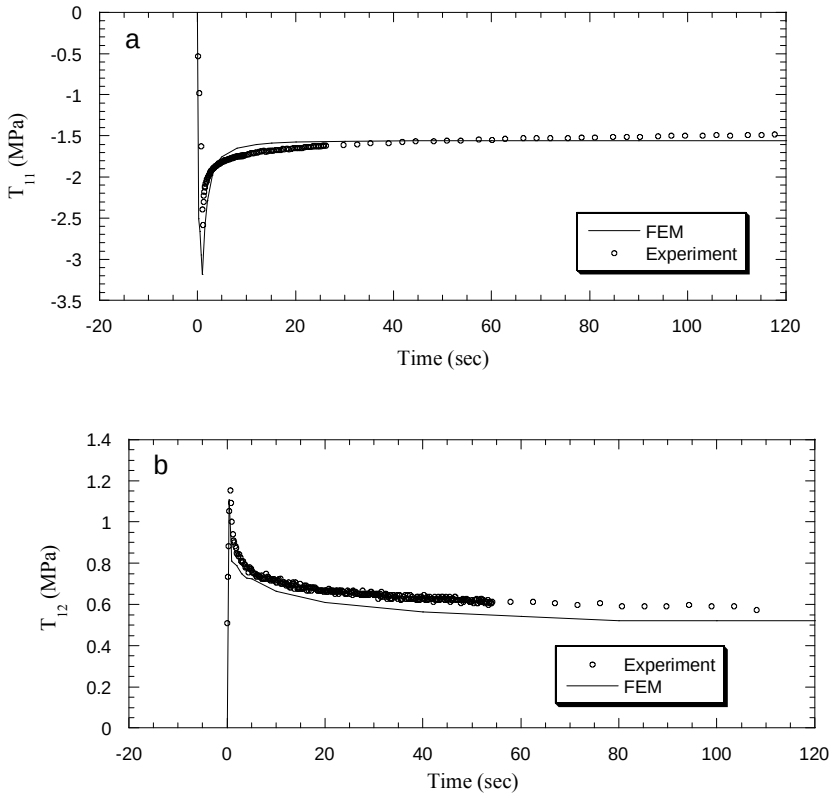

Figure 6. Numerical simulation of stress relaxation phenomena of high damping rubber under compression and shear (a) at $\lambda_1 = 0.5$; (b) at $\gamma = 1.00$ for the Mesh 1 and Mesh 2, respectively (Fig 1).

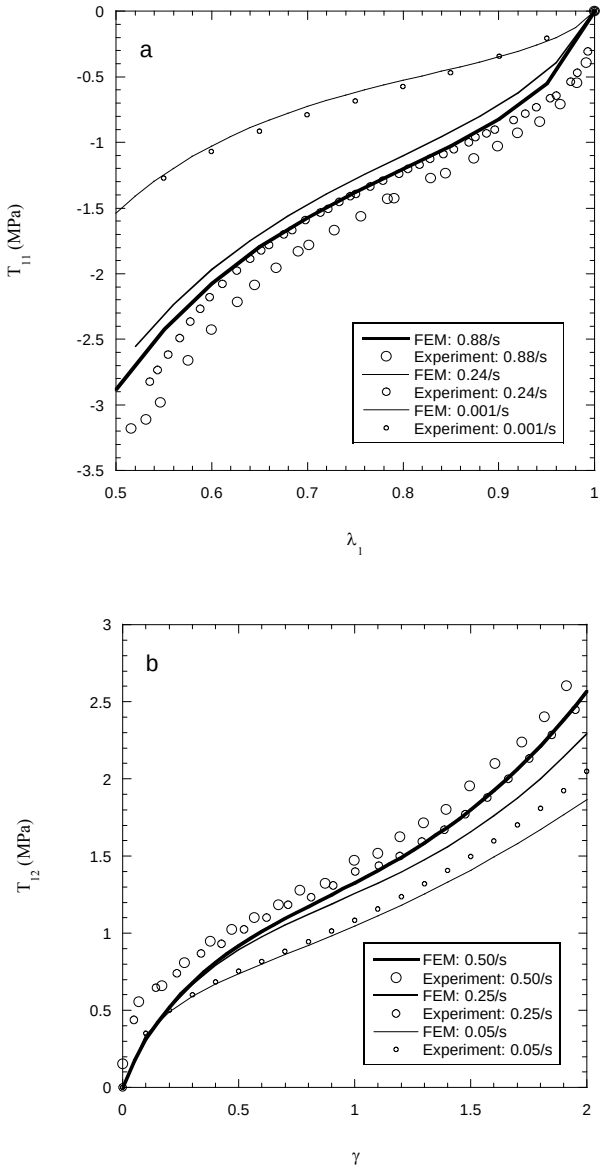

Figure 7. Simulation of strain-rate dependency effects on rubber blocks and comparison with experiments in high damping rubber. (a) Simulation of monotonic compression experiments at different strain-rates using Mesh 1. (b) Simulation of simple shear experiments at different strain-rates using Mesh 2.

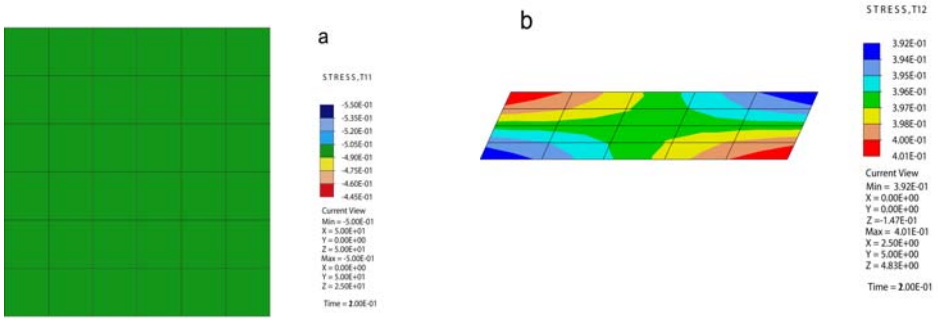

Figure 8. Numerical simulation of stress response obtained from high damping rubber (a) Stress contours obtained using Mesh 1 under uniaxial homogeneous compression, $\lambda_1 = 0.9$, $\dot{\lambda}_1 = 0.001/s$, (b) Stress contours obtained using Mesh 2 under simple shear, $\gamma = 0.20$, $\dot{\gamma} = 0.05/s$. Stress is in MPa.

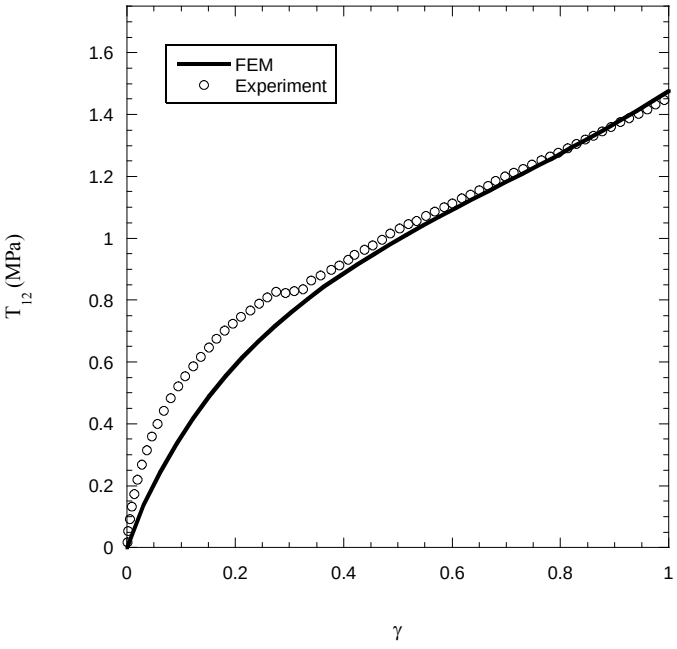

Figure 9. Comparison of simulation results with experiments obtained in a high damping rubber bearing (after, Bhuiyan et al. 2009). Bearing dimension: l_a : $240mm$, l_b : $240mm$, t_r : $5mm$, t_s : $2mm$, n_r : 6, n_s : 5, h : $40mm$, shape factor 12. Applied strain rate, $\dot{\gamma} = 1.5/s$. Mesh 3 with 92 elements was used in simulation. $Shape\ \ factor = l_a l_b / 2t_r(l_a + l_b)$.

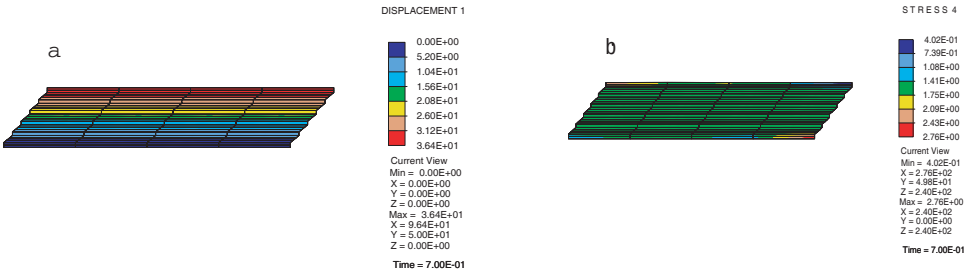

Figure 10. Numerical simulation of stress response obtained from high damping rubber bearing (Fig. 6). (a) Displacement contours and (b) Stress contours at $\gamma = 1.2$, $\dot{\gamma} = 0.75/s$. Stress is in MPa. Mesh 3 with 92 elements was used in simulation.

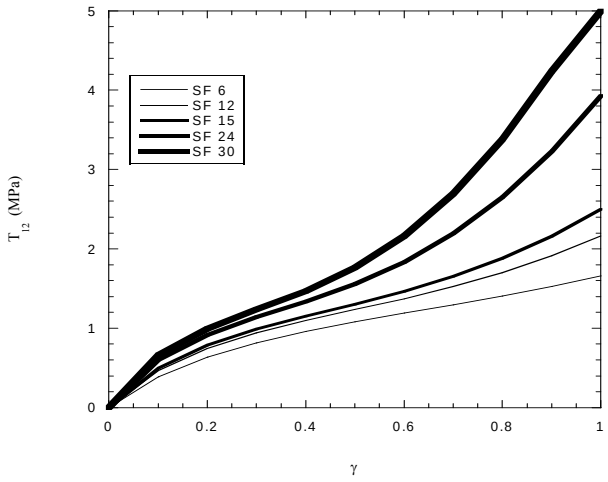

Figure 11. Effect of shape factor on the shear stress, T_{12} - shear strain, γ response of the bearing.

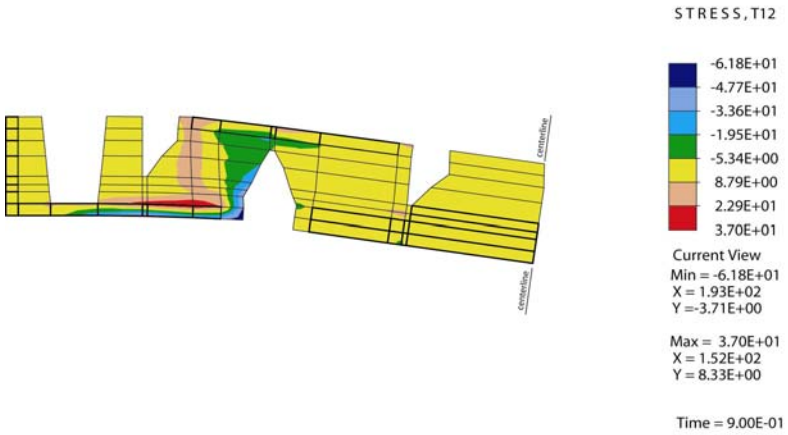

Figure 12. T_{12} contour in the expansion joint (Figs 2 and 3) obtained via finite element simulation. The contour is superimposed on the deformed mesh. Loading condition: Total uniformly distributed load in vertical direction: 150 kN and differential shear strain, $\gamma = 0.05$ applied at a strain rate of 1/s between the two ends. The applied shear strain corresponds to the displacement due to vertical reaction forces. The location of stress concentration is visible. Material data follow from Tables 1 and 2 as the exact type of rubber used there and corresponding material parameters are not available today. Stress is in MPa.